PAPER

Phase response of atom interferometers based on sequential Bragg diffractions

IOP ebooks™

Bringing you innovative digital publishing with leading voices to create your essential collection of books in STEM research.

Start exploring the collection - download the first chapter of every title for free.

Phase response of atom interferometers based on sequential Bragg diffractions

B Décamps, M Bordoux, J Alibert, B Allard and A Gauguet

Laboratoire Collision Agrégats Réactivité, IRSAMC, Université de Toulouse, CNRS, UPS, Toulouse, France

E-mail: gauguet@irsamc.ups-tlse.fr

Abstract
Large momentum transfer (LMT) beam splitters are implemented in atom interferometers to increase their sensitivity. However, an LMT interferometer requires additional light pulses to modify the response function of the atom interferometer. In this paper, we develop an analytical model for the sensitivity function of LMT interferometers using sequential accelerating light pulses. We use the sensitivity function to calculate the acceleration sensitivity taking into account the pulse duration. In addition, the sensitivity to laser phase fluctuations is calculated, and we show that the pulse sequence can be engineered to mitigate the phase noise sensitivity.

Keywords: atom interferometry, large momentum beam splitter, phase response function

(Some figures may appear in colour only in the online journal)

1. Introduction

Light-pulse atom interferometers [1] are implemented for precision measurements in various areas [2]. In particular, they have been used for gravito-inertial measurements such as the Earth's gravitation [3–5], its gradients [6], and rotations [7–9]. They are also used for measuring fundamental constants such as the gravitational constant [10, 11] or the fine structure constant [12, 13]. In addition, atom interferometers with an increased sensitivity are potential candidates for laboratory tests of general relativity [14], the weak equivalence principle [15–18], abnormal acceleration at various length scales [19, 20] or for the detection of gravitational waves [21]. In order to increase their sensitivity, a promising idea is to increase the momentum separation between the two arms of the interferometer.

Various solutions have been developed to implement large momentum transfer (LMT) beam splitters in an atom interferometer: either by using a multiphoton transition with a single pulse [22], or by using a beam splitter pulse ($\pi/2$-pulse) followed by an acceleration of the interferometer arms. The acceleration can be controlled by an optical lattice (Bloch) [23, 24] or can result from a sequence of light pulses (π-pulse) [25]. These additional light pulses change the interferometer phase, which is why an accurate model of the response functions of the LMT atom interferometer is required for precision measurements. Phase shift calculations for arbitrary atom

interferometer geometries have been studied extensively [26–29]. However, most of these methods are not convenient for modeling precisely the laser phase evolution experienced by the atoms during the light pulses.

In this paper, we calculate the response function of an LMT interferometer based on the sequential light pulse acceleration. The calculation relies on the sensitivity function formalism, initially developed for atomic clocks [30], which proved to be very efficient in the analysis of the sensitivity of light-pulse atom interferometers thereafter [31]. In particular, this formalism can precisely calculate the impact of phase fluctuations at any frequency. It is also used to determine the modification of the interferometer space-time area due to the finite duration of the light pulses. A straightforward extension of this formalism can model any interferometer involving two quantum states. However, LMT interferometers based on sequential accelerating pulses couple more than two momentum states. In this paper, we extend the sensitivity function formalism to these LMT interferometers and we derive an analytical solution for the response function in the temporal and Fourier domains. The paper is structured as follows: in section 2 we describe the atom interferometer modeled in this paper, in section 3 we introduce the sensitivity function of this type of interferometer, and in section 4 we calculate the spectral response to evaluate phase noise contributions, emphasizing the specific features of the sequential LMT interferometers.
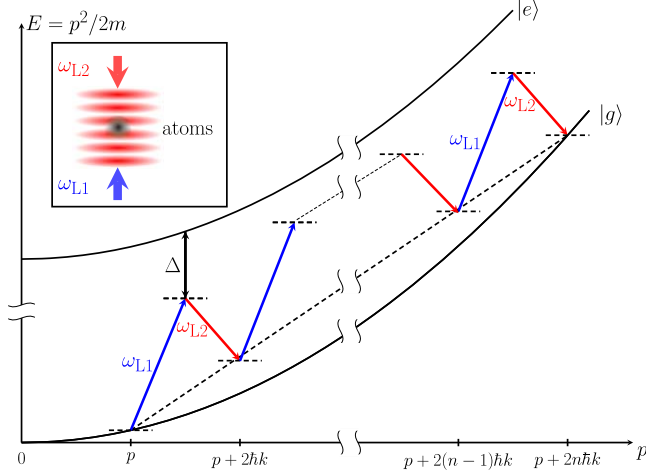
Figure 1. High-order Bragg diffraction. The multiple interactions with the two far detuned Bragg beams at frequency ω_{L1} and ω_{L2} couple the momentum states $|g, \mathbf{p}\rangle$ and $|g, \mathbf{p} + 2n\hbar\mathbf{k}\rangle$. The diffraction order n is set by the tuning of the laser frequencies. Δ is the single photon detuning with respect to the excited state $|e\rangle$. Inset: counter-propagative Bragg configuration.
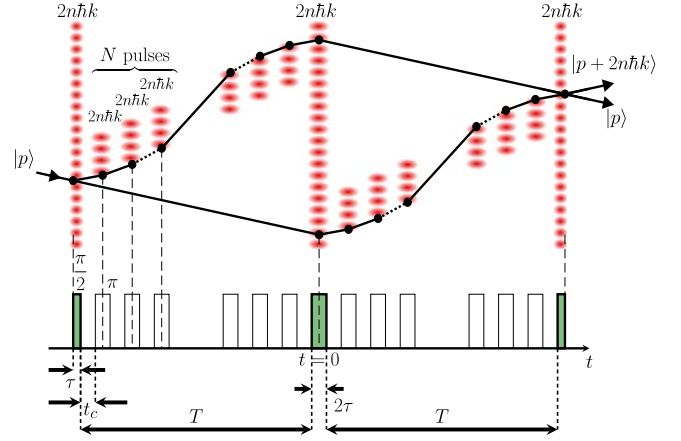
2. The LMT atom interferometer

We consider LMT atom interferometers based on sequential Bragg pulses. The Bragg lattices are created by two counter-propagative laser beams with adjustable frequencies ω_{L1} and ω_{L2} (see inset of figure 1), and the phase difference between the two lasers is labelled ϕ in the following. The detuning Δ of the two beams with respect to the single-photon transition is large compared to the excited state line-width to avoid any spontaneous emission.

Here, we consider high-order Bragg diffraction pulses that couple momentum states with a momentum separation of $2n\hbar\mathbf{k}$, where the order of diffraction n is an integer number and $\mathbf{k}$ is the laser wave-vector. The high-order Bragg coupling, illustrated in figure 1 in the laboratory frame, can be modeled as an effective coupling between two momentum states $|\mathbf{p}\rangle$ and $|\mathbf{p} + 2n\hbar\mathbf{k}\rangle$. For a square pulse, the effective Rabi frequency between those two states Ω_R is a function of the two-photon Rabi frequency Ω_0 and the diffraction order n [32]:

$$\Omega_R = \frac{\Omega_0^n}{[(n-1)!]^2} \frac{1}{(8\omega_r)^{n-1}}, \tag{1}$$

where $\omega_r = \frac{\hbar \mathbf{k}^2}{2m}$ is the recoil frequency for an atom of mass m. The relevance of this equation is questionable for high n. However, it illustrates that the required laser intensity increases rapidly with the Bragg order n. In addition, for an nth order Bragg transition, the laser phase imprinted on the diffracted state $|\mathbf{p} + 2n\hbar\mathbf{k}\rangle$ is $n \times \phi$.

The atom interferometer considered is based on a Mach–Zehnder geometry as shown in figure 2. It consists of a series of three diffracting Bragg pulses that act on both arms of the interferometer. The input state of the interferometer is $|\mathbf{p}\rangle$. A first $\pi/2$-pulse of duration τ creates a coherent superposition of the two momentum states $|\mathbf{p}\rangle$ and $|\mathbf{p} + 2n\hbar\mathbf{k}\rangle$. After a time T, a central π-pulse of duration 2τ exchanges the momentum

Figure 2. The upper panel represents the space-time diagram of the considered LMT interferometer in the Bragg lattice frame. The three long red lattices are the diffracting $\pi/2$-π-$\pi/2$-pulses of a standard Mach–Zehnder atom interferometer with a $2T$ interrogation time. The space-time area is increased by sequences of N accelerating π-pulses separated by a time t_c, acting only on a single arm (short red lattices). Each nth order Bragg pulse lasts τ (resp. 2τ) for $\pi/2$-pulses (resp. π-pulses). The lower panel sketches the intensity of the Bragg beams as a function of time.

of the two arms. Finally, after another time T, the last $\pi/2$-pulse closes the interferometer paths. Those diffracting pulses are illustrated in figure 2 by long red lattices.

To increase the momentum separation between the two interferometer arms, accelerating pulses are resonant with only one of the interferometer arms at a time. After the first diffracting pulse, a first sequence of N π-pulses of duration 2τ transfers $N \times 2n\hbar\mathbf{k}$ to the upper arm. The accelerating pulses are regularly separated by a time t_c. For simplicity, we consider that the delay between the end of the first diffracting $\pi/2$-pulse and the first accelerating pulse is t_c. A second sequence of N π-pulses decelerates the upper arm down to $|\mathbf{p} + 2n\hbar\mathbf{k}\rangle$ before the central diffracting π-pulse. It is important to note that each accelerating pulse of the first sequence has its symmetric decelerating pulse in the second sequence. The same acceleration-deceleration sequence is applied to the lower arm after the central π-pulse.

The interferometric signal corresponds to the probability of finding the atoms in either state at the output port of the interferometer. It is determined from the atomic populations measured in each interferometer output:

$$P = \frac{N_{|\mathbf{p}\rangle}}{N_{|\mathbf{p}+2n\hbar\mathbf{k}\rangle} + N_{|\mathbf{p}\rangle}} = \frac{1 + \cos\Phi}{2}, \tag{2}$$

with Φ the phase difference between the two arms that contain the signal of interest. In many cases, the measured phase shift Φ is proportional to the effective momentum separation $\mathbf{k}_{\text{eff}} = 2n(N + 1)\mathbf{k}$.

With uncorrelated atoms, the smallest measurable phase shift (the phase sensitivity) is ultimately limited by the quantum projection noise that scales with the square root of the detected atom number [33]. In practice, the phase sensitivity is lowered by laser phase noises that can be evaluated with the sensitivity function.

J. Phys. B: At. Mol. Opt. Phys. **52** (2019) 015003

B Décamps *et al*

3. Sensitivity function

An infinitesimal laser phase shift between the two lasers of the Bragg lattice $\delta\phi$ modifies the atom interferometer phase shift Φ and so the population measured at the interferometer outputs. The sensitivity function corresponds to the phase response of the interferometer for a laser phase shift $\delta\phi$ occurring at time t. The sensitivity function $g_\phi(t)$ of the interferometer is defined by:

$$g_\phi(t) := \lim_{\delta\phi\to 0} \frac{\delta\Phi(\delta\phi, t)}{\delta\phi} = \frac{2}{\sin\Phi} \lim_{\delta\phi\to 0} \frac{\delta P(\Phi, \delta\phi, t)}{\delta\phi}. \quad (3)$$

This function is used to determine the interferometric phase shift Φ for a laser phase fluctuation $\phi(t)$ during the interferometer sequence:

$$\Phi = \int_{-\infty}^{+\infty} g_\phi(t') \frac{d\phi}{dt}(t')dt'. \quad (4)$$

Our calculation of the sensitivity function relies on three main assumptions. First, we model each multiphoton transition with an effective coupling between only two states. Second, the square light pulses considered are resonant with the effective transition. Third, the interferometer is operated at its maximal sensitivity $\Phi \sim \pi/2$.

3.1. Sensitivity function for a three-pulses interferometer

The sensitivity function of the standard three-pulses interferometer has been calculated in [31] for the effective two-levels system associated with a two-photon Raman transition [34]. Their results can be directly adapted to any effective two-level system. In particular, we consider the coupling between two momentum states for an atom in an optical lattice in the Bragg regime. The sensitivity function $g_\phi^{(0)}(t)$ is an odd function of time so it is completely determined for $t \geqslant 0$:

$$g_\phi^{(0)}(t) = \begin{cases} n \times \sin(\Omega_R t) & t \in [0; \tau] \\ n & t \in [\tau; T + \tau] \\ -n \times \sin(\Omega_R(T - t)) & t \in [T + \tau; T + 2\tau] \end{cases}. \quad (5)$$

The sensitivity function is plotted in figure 3 for an interferometer with momentum separation of $36\hbar k$ using high order Bragg diffraction ($n = 18$).

3.2. Sensitivity function for a sequential LMT-interferometer

This paper focuses on the extension of the previous formalism in order to include the phase shift induced by the additional accelerating light pulses. The calculation of the sensitivity function for a sequential LMT-interferometer $g_\phi^{(LMT)}$ is detailed in the appendix. The derivation is based on the separation of $g_\phi^{(LMT)}$ into a discrete sum of terms with different starting times and durations (see figure 4).

The first term $g_0(t)$ corresponds to the sensitivity function of the diffracting pulses ($\pi/2 - \pi - \pi/2$) interacting with the two arms of the interferometer. With our choice of timings (total duration from the first pulse to the last pulse equals to
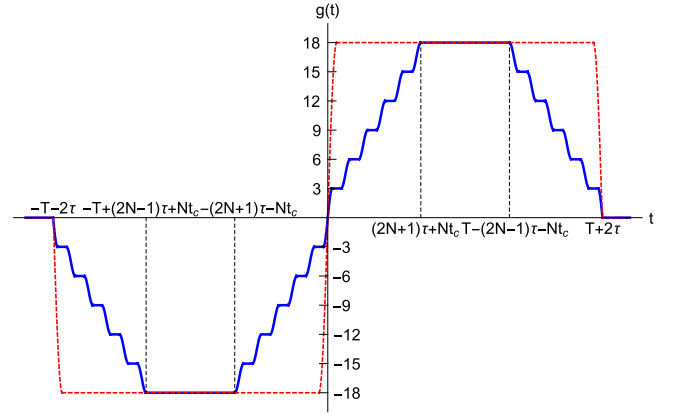
Figure 3. Sensitivity functions of a three-pulse interferometer (dashed red) and an N = 5 LMT interferometer (continuous blue). In order to compare similar scaling factors, the diffraction order is $n = 18$ for the three-pulse interferometer and $n = 3$ for the LMT-interferometer sequence.
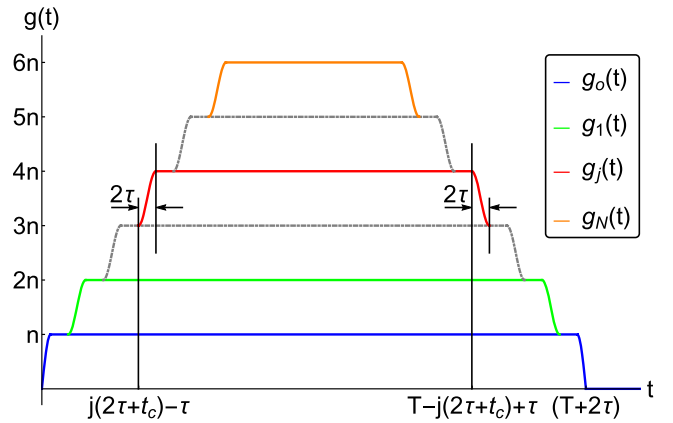
Figure 4. Representation of the partial sensitivity function as defined in equation (7) for $N = 5$. The timing of the jth pulse (continuous red line) as well as the end of the final pulse are indicated on the temporal axis.

$2(T + 2\tau)$) it is equal to the three-pulse sensitivity function:

$$g_0(t) = g_\phi^{(0)}(t). \quad (6)$$

We define a sensitivity function $g_j(t)$ for each pair of accelerating and decelerating pulses between the momentum states $j \times 2n\hbar\mathbf{k}$ and $(j + 1) \times 2n\hbar\mathbf{k}$ and we find that:

$$g_j(t) = \begin{cases} 0 & t \in [0; t_{j1}] \\ n \times \sin\left(\frac{\Omega_{\text{eff}}(t - t_{j1})}{2}\right)^2 & t \in [t_{j1}; t_{j2}] \\ n & t \in [t_{j2}; t_{j3}] \\ n \times \sin\left(\frac{\Omega_{\text{eff}}(t_{j4} - t)}{2}\right)^2 & t \in [t_{j3}; t_{j4}] \\ 0 & t \in [t_{j4}; T + 2\tau] \end{cases}. \quad (7)$$

The jth accelerating pulse after the diffracting π-pulse starts at $t_{j1} = j(2\tau + t_c) - \tau$ and ends at $t_{j2} = j(2\tau + t_c) + \tau$, it is combined with the jth decelerating pulse which

J. Phys. B: At. Mol. Opt. Phys. **52** (2019) 015003

B Décamps *et al*

starts at $t_{j3} = T - j(2\tau + t_c) + \tau$ and ends at $t_{j4} = T - j(2\tau + t_c) + 3\tau$. The global sensitivity function is then

$$g_\phi^{(LMT)}(t) = \sum_{k=0}^{N} g_j(t). \tag{8}$$

The sensitivity function for an LMT interferometer with a momentum separation of $36\hbar k$ is shown in figure 3 in the case of $N = 5$ and $n = 3$.

3.3. The acceleration scale factor

The phase shift of an LMT interferometer can be calculated from a deterministic laser phase evolution $\phi(t)$ experienced by the atom by integrating the sensitivity function (4). We consider atomic motion described by a constant acceleration $\mathbf{a}_c$ in the laboratory frame. Therefore an atom moving in the laser lattice experiences a laser phase evolution given by:

$$\frac{d\phi(t)}{dt} = 2\,\mathbf{k}\cdot\mathbf{a_c}\,t + 2\frac{\mathbf{k}\cdot\mathbf{p}}{m}. \tag{9}$$

In practice, the frequency difference between the lasers is adjusted to retain the Bragg resonance condition during all the light pulses, according to the assumption made for the calculation. One can compute directly the phase resulting from the constant acceleration which accounts for the finite duration of the light pulses. As the sensitivity function is antisymmetric, the integral over $g_\phi(t)p$ vanishes, which means that this atom interferometer geometry is independent of the initial atom momentum $\mathbf{p}$. The phase shift obtained for a three-pulse sequence ($N = 0$) is:

$$\frac{\Phi_{acc,3}}{\mathbf{k}_{eff}\cdot\mathbf{a}_c T^2} = 1 + \left(1 + \frac{2}{\pi}\right)\frac{2\tau}{T} + \frac{2}{\pi}\left(\frac{2\tau}{T}\right)^2. \tag{10}$$

The phase shift obtained for LMT interferometer is:

$$\frac{\Phi_{acc}}{\mathbf{k}_{eff}\cdot\mathbf{a}_c T^2} = 1 + \left(1 + \frac{2}{\pi} - N(N-1)\right)\frac{1}{N+1}\frac{2\tau}{T} - N\frac{t_c}{T} \\ + \left(\frac{2}{\pi} + N\right)\frac{1}{N+1}\left(\frac{2\tau}{T}\right)^2 . \tag{11}$$

In order to compare the sensitivity between the N-pulse and the standard three-pulse interferometers, we consider identical pulse durations (τ) and an identical total momentum transfer $\mathbf{k}_{eff}$. In the limit of infinitely short light pulses (t_c, $\tau \to 0$), we find the expected factor which scales as the momentum difference and the interferometric time squared $k_{eff}T^2$. However, precision measurements need an accurate knowledge of the scale factor which requires us to consider the additional terms in τ/T and t_c/T. In the case of the LMT sequence, momentum transfer takes a longer duration than the equivalent three-pulse interferometer and this slightly modifies the space-time area:

$$\frac{\Phi_{acc,3} - \Phi_{acc}}{\mathbf{k}_{eff}\cdot\mathbf{a}_c T^2} = \frac{N}{N+1}\left(\frac{2}{\pi} + N\right)\frac{2\tau}{T} + N\frac{t_c}{T} \\ - \frac{N}{N+1}\left(1 - \frac{2}{\pi}\right)\left(\frac{2\tau}{T}\right)^2 . \tag{12}$$

4. Phase noise sensitivity

To estimate the impact of the laser phase noise on the interferometer sensitivity, it is convenient to define the transfer function of the interferometer in the Fourier domain $H(\omega)$. The variance of the interferometric phase is given by the power spectral density $S_\phi(\omega)$ of the laser phase noise weighted by the transfer function:

$$\sigma_\Phi^2 = \int_0^\infty |H(\omega)|^2 S_\phi(\omega)\frac{d\omega}{2\pi}. \tag{13}$$

With the transfer function of the interferometer $H(\omega)$ defined as:

$$H(\omega) := \omega \int_{-\infty}^{+\infty} e^{-i\omega t} g_\phi(t)dt. \tag{14}$$

To determine $H(\omega)$, we define the partial transfer function for each individual partial sensitivity function $g_j(t)$:

$$H_j(\omega) := \omega \int_{-\infty}^{+\infty} e^{-i\omega t} g_j(t)dt. \tag{15}$$

From the equations (7) and (15) we calculate each partial transfer function. For $j = 0$, we recover the usual three-pulse transfer function [31]:
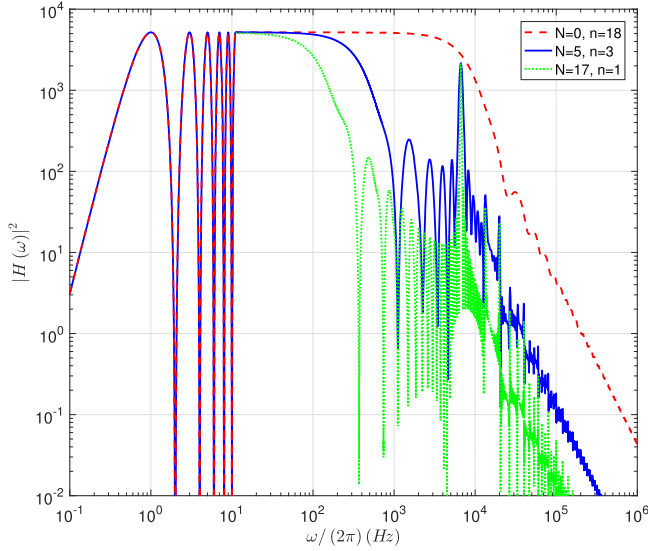
$$H_0(\omega) = \frac{4in\Omega_R^2}{\omega^2 - \Omega_R^2}\sin\left(\omega\frac{T+2\tau}{2}\right) \\ \times\left\{\sin\left(\omega\frac{T}{2}\right) + \frac{\omega}{\Omega_R}\cos\left(\omega\frac{T+2\tau}{2}\right)\right\}. \tag{16}$$

For $j \neq 0$, the partial transfer function is given by:

$$H_j(\omega) = \frac{4in\Omega_R^2}{\omega^2 - \Omega_R^2}\sin\left(\omega\frac{T+2\tau}{2}\right) \\ \times\sin\left(\omega\frac{T-2j(2\tau+t_c)+2\tau}{2}\right)\cos(\omega\tau). \tag{17}$$

The transfer function of the interferometer $H(\omega)$ is the sum of all the partial transfer functions. First we calculate the sum $\sum_{j=1}^{N} H_j(\omega)$, dropping the global factor independent on j, one gets:

$$\sum_{j=1}^{N} H_j \propto \sum_{j=0}^{N-1}\sin\left(\omega\frac{T-2(\tau+t_c)+j(-4\tau-2t_c)}{2}\right). \tag{18}$$

J. Phys. B: At. Mol. Opt. Phys. **52** (2019) 015003

B Décamps *et al*

Figure 5. Transfer functions $|H(\omega)|^2$ of a three-pulse (red dashed line), $N = 5$ multipulse (blue solid line) and $N = 17$ multipulse (green dashed-dotted line), for $2T = 500\,ms$, $\tau = 50\,\mu s$ and $\tau_c = 50\,\mu s$.

This expression is simplified with the following property [35]:

$$\sum_{j=0}^{N-1} \sin(x + jy) = \frac{\sin\left(x + \frac{(N-1)y}{2}\right)\sin\left(\frac{Ny}{2}\right)}{\sin\left(y/2\right)}. \tag{19}$$

Finally, we get the global transfer function of the atom interferometer, which is the central result of this paper:

$$H(\omega) = \frac{4in\Omega_R^2}{\omega^2 - \Omega_R^2}\sin\left(\omega\frac{T + 2\tau}{2}\right)$$
$$\times\left\{\frac{\omega}{\Omega_R}\cos\left(\omega\frac{T + 2\tau}{2}\right) + \sin\left(\omega\frac{T}{2}\right)\right.$$
$$+ \frac{\sin\left(\omega\frac{N(t_c + 2\tau)}{2}\right)}{\sin\left(\omega\frac{t_c + 2\tau}{2}\right)}\cos(\omega\tau) \tag{20}$$
$$\left.\times\sin\left(\omega\frac{T - (N + 1)t_c - 2N\tau}{2}\right)\right\}$$

In figure 5, we plot $|H(\omega)|^2$ for three interferometers of identical space-time area ($2T = 500\,ms$, and $36\,\hbar k$). We consider a three-pulse interferometer with high-order Bragg pulses $n = 18$ (red dashed line), an LMT interferometer with first-order Bragg pulses $n = 1$ and many accelerating pulses $N = 17$ (green dashed-dotted line) and an intermediate configuration with $N = 5$ and $n = 3$ (blue solid line). In addition, we keep the pulse duration $\tau = 50\,ms$, and the pulse delay $t_c = 50\,\mu s$ identical for the three configurations.

At low frequency ($\omega/(2\pi) < (2N + 1)/(2T)$), $|H(\omega)|^2$ does not depend on the specific sequence of the beam splitters. In particular, the finite duration $2T$ of the interferometer induces periodic cancellation at frequencies of $1/(T + 2\tau)$ (2 Hz with our parameters). This feature is shown in figure 5
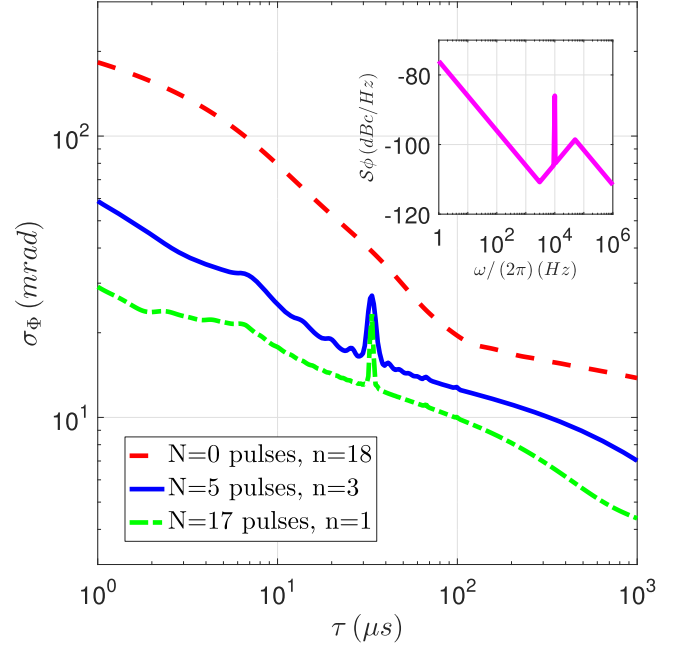
Figure 6. Interferometer phase noise from equation (13) for different diffracting pulses durations. The interferometric time is constant ($2T = 500\,ms$) and for simplicity, the delay between each pulse is chosen to be equal to the pulse duration ($t_c = \tau$). The phase power spectrum density used is shown as an inset. Different interferometer configurations are considered ($N = 0$, red dashed line; $N = 5$, blue solid line; and $N = 17$, green dot-dashed line.)

at low frequencies ($f < 11$ Hz). At higher frequencies (>11 Hz), we plot the averaged value of $|H(\omega)|^2$ over a $1/T$ frequency span for a better readability of its envelope. Besides, a numerical factor multiplies the averaged plots to match the low frequency maxima obtained without averaging.

The finite duration of the pulses leads to a low-pass filtering with a $1/f^2$ scaling which is characteristic of rectangular pulses [36]. In the case of the three-pulse interferometer the cut-off frequency is $\sim 1/(2\tau)$ (10 kHz with our parameters). For the LMT-interferometer, the effective duration of the beam splitter leads to a lower cut-off frequency $\sim(2N \times (2\tau + t_c))^{-1}$. Moreover, it is interesting to note that, regardless of the partial cancellation of sensitivity to frequencies above the effective cutoff, a residual phase sensitivity around $\omega/(2\pi) \sim 1/(2\tau + t_c)$ remains independent of the number of intermediate pulses.

In order to illustrate the impact of the pulse sequence, we modeled a laser phase noise characterized by the power spectral density $S_\phi(\omega)$ shown in the inset of figure 6. In this example, we considered phase-locked lasers shifted by a few MHz for Bragg diffraction. The phase noise is representative of an optical phase locked loop limited by the finite bandwidth of acousto-optic modulators used for the feedback (~ 50 kHz in our example). Figure 6 shows the laser phase noise according to the pulse duration τ for the three interferometer configurations ($N = 0$, $N = 5$ and $N = 17$). It emphasizes the decrease in phase noise reachable in a multipulse configuration due to the high frequency filtering. Moreover, we added a sharp resonance in the noise spectra

($f_0 = 10$ kHz in our example), which leads to an increased phase noise for a pulse duration of $\sim 1/(3f_0)$. This example shows the possibility of the developed formalism to design an optimized interferometer sequence depending on the specific technical laser phase noise and/or power limitation.

5. Conclusion

We derived the response function of a light-pulse atom interferometer using a sequential diffraction in the temporal and Fourier domains. The model presented in this paper is based on sequential effective two-level couplings, hence it can be extended to the other sequential light pulses such as two-photon Raman transition or single-photon transition. The precise knowledge of this transfer function allows us to calculate the influence of several noise contributions onto the

$$
\begin{pmatrix}
\cos\left[\dfrac{\Omega_R(t_f - t)}{2}\right]e^{-i\omega_j(t_f - t)} & -ie^{i(\omega_{12}t + n\phi)}\sin\left[\dfrac{\Omega_R(t_f - t)}{2}\right]e^{-i\omega_j(t_f - t)} \\
-ie^{-i(\omega_{12}t + n\phi)}\sin\left[\dfrac{\Omega_R(t_f - t)}{2}\right]e^{-i\omega_{j+1}(t_f - t)} & \cos\left[\dfrac{\Omega_R(t_f - t)}{2}\right]e^{-i\omega_{j+1}(t_f - t)}
\end{pmatrix}
\tag{A.1}
$$

atom interferometers. In particular, we highlighted resonances in the transfer function depending on the sequence of the LMT beam splitters. In addition, a central result of our study is the rejection of high frequency laser phase fluctuations for sequential pulse LMT beam splitters. The modification of the response function is also of great interest for implementing an active noise rejection with an external vibration sensor. We also presented the modification of the space-time area of the interferometer which impacts on the scale factor of the inertial sensor. Future work should implement the combination of pulse shaping [36] and the multipulses configuration studied in this paper, which would be directly applicable to future experiments using sequential LMT interferometers. Finally, the sensitivity function can be used for the analysis of systematic effects induced by the light pulses including light-shift which are of importance for LMT interferometers. It would be of interest to consider the case of nonresonant accelerating pulses and the effect of multiphoton light shifts [37] during the acceleration pulses.

Appendix. Detailed derivation of the sensitivity function

To compute the sensitivity function of the LMT interferometer we use a formalism based on a matrix formulation of the momentum state superposition during the interferometer sequence. For an N-pulse sequence, we consider momentum states $\{|j\rangle := |\mathbf{p} + j \times 2n\hbar\mathbf{k}\rangle\}_{j\in[0,N]}$ where $\mathbf{p}$ is the initial atomic momentum. From an initial wave function $|\Psi_0\rangle = |0\rangle$ one can compute the atomic wave function evolution by considering a sequence of light pulses coupling only neighboring states and leaving the other states evolving freely. Each step can be represented by a matrix M_j which is block diagonal with a unique 2×2 irreducible subspace coupling $|j\rangle$ and $|j + 1\rangle$ expressed as:

where $\Omega_R/(2\pi)$ is the Rabi frequency, $\hbar\omega_j$ is the energy of the state $|j\rangle$, $\omega_{12} = \omega_{L1} - \omega_{L2}$ is the frequency difference between the two counter-propagating lasers, t is the absolute timing at the start of the time step, ϕ is the laser phase at this instant and t_f is the time at the end of the step. All other nonzero elements of M_j lie on the diagonal and are simply $\{e^{-i\omega_q(t_f - t)}\}_{q\neq j,j+1}$. The interferometric sequence is then directly represented by a product of $5 + 8N$ of these matrices (see figure A1). These matrices depend on four parameters: the initial time t, the Rabi frequency Ω_R, the pulse duration $t_f - t$, and the laser phase difference ϕ. As an example, the N = 1 sequence corresponds to:

$$
\begin{aligned}
&M_0^{XIII}(T + \tau, \Omega_R, \tau, \phi_3).M_p^{XII}(T + \tau - t_c, t_c) \\
&\quad .M_1^{XI}(T - \tau - t_c, \Omega_R, 2\tau, \phi_2). \\
&M_p^{X}(3\tau + t_c, T - 4\tau - 2t_c).M_1^{IX}(\tau + t_c, \Omega_R, 2\tau, \phi_2) \\
&\quad .M_p^{VIII}(\tau, t_c).M_0^{VII}(-\tau, \Omega_R, 2\tau, \phi_2). \\
&M_p^{VI}(-\tau - t_c, t_c).M_1^{V}(-3\tau - t_c, \Omega_R, 2\tau, \phi_1) \\
&\quad .M_p^{IV}(-T + \tau + t_c, T - 4\tau - 2t_c). \\
&M_1^{III}(-T - \tau + t_c, \Omega_R, 2\tau, \phi_1).M_p^{II}(-T - \tau, t_c) \\
&\quad .M_0^{I}(-T - 2\tau, \Omega_R, \tau, \phi_1)
\end{aligned}
\tag{A.2}
$$

where the matrices are labelled with roman numerals. For the light pulses matrices (M_0, M_1) the quadruplets $(t, \Omega_R, (t_f - t), \phi)$ are specified. During the free evolution $(\Omega_R = 0)$ the matrices (M_p) are determined by the doublets $(t, (t_f - t))$. In this expression, we have used the usual convention of setting the phase of the three-pulse interferometer to $\phi_{1,2,3}$. For clarity, we give also the full expression of the two matrices:
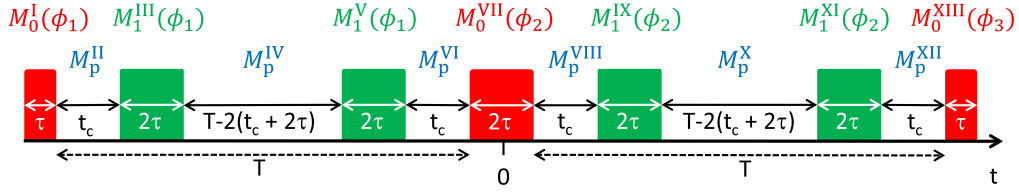
Figure A1. Complete pulse sequence including the associated matrices for $N = 1$. Red pulses correspond to the common diffracting pulses while green pulses correspond to accelerations produced on a single interferometric arm.
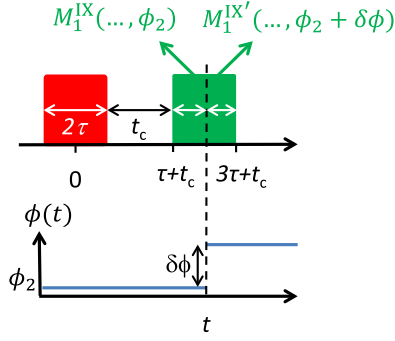
Figure A2. Schematic representation of the phase jump $\delta\phi$ happening at time t during the IXth step. The associated matrix is split into two halves which depend on t.

on the time at which the step occurs, the corresponding matrix into two matrices with different laser phases (only relevant when $\Omega_R \neq 0$). For example (see figure A2), if the phase step happens during the interval $[t_c + \tau; t_c + 3\tau]$, one has to replace the term $M_1^{IX}(t_c + \tau, \Omega_R, 2\tau, \phi_2)$ by the product:

$$M_1^{IX'}(t, \Omega_R, 3\tau + t_c - t, \phi_2 + \delta\phi)$$
$$\times .M_1^{IX}(\tau + t_c, \Omega_R, t - (\tau + t_c), \phi_2) \qquad (A.4)$$

and propagate the additional phase $\delta\phi$ in all subsequent laser phases present in later matrices. This results in an additional accumulated phase $\delta\Phi(\delta\phi, t)$ which directly gives the sensitivity function with:

$$g_\phi(t) = \lim_{\delta\phi \to 0} \frac{\delta\Phi(\delta\phi, t)}{\delta\phi} \qquad (A.5)$$

$$M_0 = \begin{pmatrix} \cos\left[\dfrac{\Omega_R(t_f - t)}{2}\right]e^{-i\omega_0(t_f-t)} & -ie^{i(\omega_{12}t+n\phi)}\sin\left[\dfrac{\Omega_R(t_f - t)}{2}\right]e^{-i\omega_0(t_f-t)} & 0 \\ -ie^{-i(\omega_{12}t+n\phi)}\sin\left[\dfrac{\Omega_R(t_f - t)}{2}\right]e^{-i\omega_1(t_f-t)} & \cos\left[\dfrac{\Omega_R(t_f - t)}{2}\right]e^{-i\omega_1(t_f-t)} & 0 \\ 0 & 0 & e^{-i\omega_2(t_f-t)} \end{pmatrix}$$

and

$$M_1 = \begin{pmatrix} e^{-i\omega_0(t_f-t)} & 0 & 0 \\ 0 & \cos\left[\dfrac{\Omega_R(t_f - t)}{2}\right]e^{-i\omega_1(t_f-t)} & -ie^{i(\omega_{12}t+n\phi)}\sin\left[\dfrac{\Omega_R(t_f - t)}{2}\right]e^{-i\omega_1(t_f-t)} \\ 0 & -ie^{-i(\omega_{12}t+n\phi)}\sin\left[\dfrac{\Omega_R(t_f - t)}{2}\right]e^{-i\omega_2(t_f-t)} & \cos\left[\dfrac{\Omega_R(t_f - t)}{2}\right]e^{-i\omega_2(t_f-t)} \end{pmatrix}.$$

The output state corresponds to a superposition of $|0\rangle$ and $|1\rangle$, from which we find the accumulated phase $\Phi^{(N)}$, given by the usual formula:

$$\Phi^{(N)} = n(N + 1)[\phi_1 - 2\phi_2 + \phi_3]. \qquad (A.3)$$

Finally, to obtain the sensitivity function (equation (3)) one has to include a step change in phase for all possible times in the interferometer sequence. This can be done by splitting, depending

where we have used the mid fringe assumption by choosing $(N = 1)$:

$$2n(\phi_1 - 2\phi_2 + \phi_3) = \frac{\pi}{2}. \qquad (A.6)$$

The general form given by equation (7) was obtained from a full calculation of resonance ($\omega_{12} = \omega_{j+1} - \omega_j \,\forall j$) for $N = 1, 2$ and 3 and then generalizing to arbitrary N using the temporal symmetry of the interferometer sequence.

ORCID iDs

A Gauguet ⬤ https://orcid.org/0000-0002-3994-8881

References

[1] Bordé C J 1989 *Phys. Lett.* A **140** 10
[2] Tino G M and Kasevich M A (ed) 2014 *Atom Interferometry* (Amsterdam: IOS Press)
[3] Louchet-Chauvet A, Farah T, Bodart Q, Clairon A, Landragin A, Merlet S and Dos Santos F P 2011 *New J. Phys.* **6** 065025
[4] Hu Z K, Sun B L, Duan X C, Zhou M K, Chen L L, Zhan S, Zhang Q Z and Luo J 2013 *Phys. Rev.* A **88** 043610
[5] Freier C, Hauth M, Schkolnik V, Leykauf B, Schilling M, Wziontek H, Scherneck H G, Müller J and Peters A 2016 *J. Phys.: Conf. Ser.* **723** 012050
[6] Sorrentino F, Bodart Q, Cacciapuoti L, Lien Y H, Prevedelli M, Rosi G, Salvi L and Tino G M 2013 *Phys. Rev.* A **89** 023607
[7] Gustavson T L, Landragin A and Kasevich M A 2000 *Class. Quantum Grav.* **17** 2385
[8] Berg P, Abend S, Tackmann G, Schubert C, Giese E, Schleich W P, Narducci F A, Ertmer W and Rasel E 2015 *Phys. Rev. Lett.* **114** 063002
[9] Barrett B, Geiger R, Dutta I, Meunier M, Canuel B, Gauguet A, Bouyer P and Landragin A 2014 *C.R. Phys.* **15** 875
[10] Fixler J B, Foster G T, McGuirk J M and Kasevich M A 2007 *Science* **315** 5808 74–77
[11] Rosi G, Sorrentino F, Cacciapuoti L, Prevedelli M and Tino G M 2014 *Nature* **510** 7506 518-521
[12] Bouchendira R, Cladé P, Guellati-Khélifa S, Nez F and Biraben F 2011 *Phys. Rev. Lett.* **106** 08080
[13] Parker R H, Yu C, Zhong W, Estey B and Müller H 2018 *Science* **360** 191–5
[14] Dimopoulos S, Graham P M, Hogan J M, Kasevich M A and Rajendran S 2008 *Phys. Rev.* D **78** 122002
[15] Zhou L *et al* 2013 *Phys. Rev. Lett.* **115** 013004
[16] Bonnin A, Zahzam N, Bidel Y and Bresson A 2013 *Phys. Rev.* A **88** 043615
[17] Barrett B, Antoni-Micollier L, Chichet L, Battelier B, Lévèque T, Landragin A and Bouyer P 2016 *Nat. Commun.* **7** 13786
[18] Overstreet C, Asembaum P, Kovachy T, Notermans R, Hogan J M and Kasevich M A 2018 *Phys. Rev. Lett.* **120** 183604
[19] Wolf P, Lemonde P, Lambrecht A, Bize S, Langevin A and Clairon A 2007 *Phys. Rev.* A **75** 063608
[20] Jaffe M, Hasslinger P, Xu V, Hamilton P, Upadhye A, Elder B, Khoury J and Müller H 2017 *Nat. Phys.* **13** 938–42
[21] Canuel B *et al* 2014 *E3S Web of Conferences* **4** 01004
[22] Müller H, Chiow S, Long Q, Herrmann S and Chu S 2008 *Phys. Rev. Lett.* **100** 180405
[23] McDonald G D, Kuhn C C N, Bennetts S, Debs J E, Hardman K S, Close J D and Robins N P 2014 *EPL* **105** 63001
[24] Cladé P, Guellati-Khélifa S, Nez F and Biraben F 2009 *Phys. Rev. Lett.* **102** 240402
[25] Chiow S, Kovachy T, Chien H C and Kasevich M A 2011 *Phys. Rev. Lett.* **107** 130403
[26] Bordé C J 2002 *Metrologia* **39** 435–63
[27] Bongs K, Launay R and Kasevich M A 2006 *Appl. Phys.* B **84** 599–602
[28] Dubetsky B and Kasevich M A 2006 *Phys. Rev.* A **74** 023615
[29] Kleinert S, Kajari E, Roura A and Schleich W P 2015 *Phys. Rep.* **605** 1–50
[30] Dick G J 1987 *Proc. XIX Ann. Precise Time and Time Interval* **19** 133
[31] Cheinet P, Canuel B, Pereira Dos Santos F, Gauguet A, Yver-Leduc F and Landragin A 2008 *IEEE Trans. Instrum. Meas.* **57** 1141
[32] Müller H, Chiow S and Chu S 2008 *Phys. Rev.* A **77** 023609
[33] Itano W M, Bergquist J C, Bollinger J J, Gilligan J M, Heinzen D J, Moore F L, Raizen M G and Wineland D J 1993 *Phys. Rev.* A **47** 3554
[34] Kasevich M A and Chu S 1992 *Appl. Phys.* B **54** 321
[35] Alan J and Hui-Hui D 2008 *Handbook of Mathematical Formulas and Integrals* 4th edn (London: Academic)
[36] Fang B, Mielec N, Savoie D, Altorio M, Landragin A and Geiger R 2018 *New J. Phys.* **20** 023020
[37] Gauguet A, Mehlstäubler T E, Lévèque T, Le Gouët J, Chaibi W, Canuel B, Clairon A, Pereira Dos Santos F and Landragin A 2008 *Phys. Rev.* A **78** 043615